Accuracies of the synthesized monochromatic CT numbers and effective atomic numbers obtained with a rapid kVp switching dual energy CT scanner

Mitchell M. Goodsitt,[a] Emmanuel G. Christodoulou, and Sandra C. Larson
Department of Radiology, University of Michigan, Ann Arbor, Michigan 48109-5842

(Received 14 September 2010; revised 23 February 2011; accepted for publication 27 February 2011; published 29 March 2011)

Purpose: This study was performed to investigate the accuracies of the synthesized monochromatic images and effective atomic number maps obtained with the new GE Discovery CT750 HD CT scanner.
Methods: A Gammex-RMI model 467 tissue characterization phantom and the CT number linearity section of a Phantom Laboratory Catphan 600 phantom were scanned using the dual energy (DE) feature on the GE CT750 HD scanner. Synthesized monochromatic images at various energies between 40 and 120 keV and effective atomic number (Z_{eff}) maps were generated. Regions of interest were placed within these images/maps to measure the average monochromatic CT numbers and average Z_{eff} of the materials within these phantoms. The true Z_{eff} values were either supplied by the phantom manufacturer or computed using Mayneord's equation. The linear attenuation coefficients for the true CT numbers were computed using the NIST XCOM program with the input of manufacturer supplied elemental compositions and densities. The effects of small variations in the assumed true densities of the materials were also investigated. Finally, the effect of body size on the accuracies of the synthesized monochromatic CT numbers was investigated using a custom lumbar section phantom with and without an external fat-mimicking ring.
Results: Other than the Z_{eff} of the simulated lung inserts in the tissue characterization phantom, which could not be measured by DECT, the Z_{eff} values of all of the other materials in the tissue characterization and Catphan phantoms were accurate to 15%. The accuracies of the synthesized monochromatic CT numbers of the materials in both phantoms varied with energy and material. For the 40–120 keV range, RMS errors between the measured and true CT numbers in the Catphan are 8–25 HU when the true CT numbers were computed using the nominal plastic densities. These RMS errors improve to 3–12 HU for assumed true densities within the nominal density ± 0.02 g/cc range. The RMS errors between the measured and true CT numbers of the tissue mimicking materials in the tissue characterization phantom over the 40–120 keV range varied from about 6 HU–248 HU and did not improve as dramatically with small changes in assumed true density.
Conclusions: Initial tests indicate that the Z_{eff} values computed with DECT on this scanner are reasonably accurate; however, the synthesized monochromatic CT numbers can be very inaccurate, especially for dense tissue mimicking materials at low energies. Furthermore, the synthesized monochromatic CT numbers of materials still depend on the amount of the surrounding tissues especially at low keV, demonstrating that the numbers are not truly monochromatic. Further research is needed to develop DE methods that produce more accurate synthesized monochromatic CT numbers. [DOI: 10.1118/1.3567509]

Key words: dual energy CT, effective atomic number, monochromatic CT number, CT number accuracy

I. INTRODUCTION

Soon after the invention of CT, dual energy methods were proposed and utilized to better discriminate and characterize tissues. In his first paper on CT published in 1973, Hounsfield[1] described the use of dual energy (DE) (e.g., subtraction of images obtained at 100 and 140 kV) to distinguish the atomic numbers of tissues. Other early pioneering works in dual energy CT (DECT) included the development of methods to measure effective atomic number and electron and mass density,[2–4] decompose measured attenuation coefficients into Compton and photoelectric components,[4,5] decompose attenuation coefficients into two basis material components and generate basis material mass density images,[6] and utilize basis material or Compton and photoelectric decomposition to synthesize monoenergetic images.[7] An important requirement for the success of dual energy CT scanning is that there should be minimal time lapse between the acquisitions of the two single energy projections/images. Otherwise, the inconsistencies that could arise (e.g., due to patient motion) would degrade the accuracies of the dual energy results and result in image artifacts. Several methods

have been utilized to meet the minimal time lapse requirement including the use of a dual detector,[8–10] a split filter,[11] a sandwiched detector,[12,13] rapid kVp switching,[14–16] and dual-source and detector scanning.[17–19]

Presently, the rapid kVp switching method and the dual-source methods are commercially available. We have a GE Discovery CT750 HD CT scanner (GE Healthcare, Milwaukee, WI) at our institution that includes their dual energy [gemstone spectral imaging (GSI)] feature. This scanner utilizes a rapid kVp switching method like the one that is described in Refs. 14–16, but with gantry rotation times of 0.5–1 s instead of 5–14 s, use of x-ray focal spot deflection, switching between 80 and 140 kVp in less than 0.5 ms instead of 10 ms, and use of a newly developed cerium activated garnet, rare-earth composite scintillator detector with 100 times faster response than a typical gadolinium oxysulfide CT detector. The system uses a dual energy prereconstruction algorithm inspired by the work of Alvarez and co-workers.[5–7] It employs proprietary basis materials and proprietary calibration methods, and computes effective atomic number maps, material density images, and synthesized monochromatic images.

The method by which the GE scanner synthesizes monochromatic CT numbers from the material density images is as follows.[20] The linear attenuation in each voxel of a monochromatic image at energy E is determined using

$$\mu(E) = d_A \cdot \frac{\mu}{\rho}(E)_A + d_B \cdot \frac{\mu}{\rho}(E)_B, \quad (1)$$

where d_A and d_B are the DECT determined densities or concentrations of basis materials A and B at the voxel location, respectively, and $(\mu/\rho)(E)_A$ *and* $(\mu/\rho)(E)_B$ are the mass attenuation coefficients of materials A and B. The corresponding monochromatic CT numbers in Hounsfield units (HU) are then computed using

$$\text{CT \# }(E) = \left[\frac{d_A \cdot (\mu/\rho)(E)_A + d_B \cdot (\mu/\rho)(E)_B - \mu(E)_{\text{water}}}{\mu(E)_{\text{water}}} \right] \cdot 1000, \quad (2)$$

where $\mu(E)_{\text{water}}$ is the linear attenuation coefficient of water at energy E and is equal to $(\mu/\rho)(E)_{\text{water}} \cdot \rho_{\text{water}}$, where ρ_{water} is the mass density of pure water.

If one of the basis materials, for example, A, is water, this equation simplifies to

$$\text{CT \# }(E) = \left[\frac{d_{\text{water}}}{\rho_{\text{water}}} - \frac{d_B}{\rho_{\text{water}}} \cdot \frac{(\mu/\rho)(E)_B}{(\mu/\rho)(E)_{\text{water}}} - 1 \right] \cdot 1000. \quad (3)$$

Monochromatic images obtained with the GE scanners have been shown to have promise in aiding the discrimination between cysts and hypodense liver metastases.[20] Monochromatic images, especially those synthesized at higher energies (e.g., 70 keV and above), display less beam hardening, scatter, and metal artifacts.

Effective atomic numbers (Z_{eff}) are determined with the GE scanner using "the monochromatic attenuation ratio method."[21] In this method, a theoretical plot of Z_{eff} as a function of the ratio of the linear attenuation coefficients at two energies (e.g., 70 and 120 keV) is employed to convert the ratio of the measured linear attenuation coefficients [e.g., obtained with Eq. (1)] at two energies to Z_{eff}. One promising application of effective atomic numbers is in distinguishing the compositions of kidney stones. In a preliminary study with the GE scanner, uric acid, cystine/struvite, and calcium based kidney stones could be determined by their locations in plots of their measured effective atomic numbers as a function of their corresponding monochromatic CT numbers at 70 keV, where the latter is a surrogate for mass density.[21]

The purpose of the present work was to evaluate the accuracies of the effective atomic numbers and the synthesized monochromatic CT numbers computed with the GE CT750 HD commercial unit.

II. MATERIALS AND METHODS

II.A. Phantoms

Three phantoms containing plastics and epoxy resin based tissue substitutes were employed as the test objects in this study. One of the phantoms was a Gammex-RMI tissue characterization phantom model 467 (Gammex Inc., Middleton, WI). This phantom was developed by Constantinou *et al.*[22] It is a 33 cm diameter cylinder made of Solid Water[23] with 16 2.8 cm holes that are filled with rod-shaped interchangeable inserts made of epoxy based tissue substitutes such as lung, cortical bone, inner bone, adipose, brain, liver, and breast.[24,25] It has also inserts made of Solid Water and one containing Liquid Water. The elemental compositions and effective atomic numbers of the inserts are listed in a paper by Bazalova.[26] The inserts were positioned in the arrangement suggested by the manufacturer in their User's Guide. The second phantom was the CT number linearity section (CTP404) of the Catphan 600 phantom (The Phantom Laboratory, Salem, NY). This section is a 20 cm diameter cylinder made of a proprietary plastic and it contains rods made of commercial plastics such as polymethylpentene (PMP), low density polyethylene (LDPE), polystyrene, acrylic, Delrin, and Teflon. The third phantom is a custom lumbar section phantom made of muscle, fat, and bone mimicking epoxy based substitutes with a hole in a simulated vertebra in which inner bone mimicking materials of known compositions can be inserted.[27] This phantom was built by CIRS, Inc. (Computerized Imaging Reference Systems, Inc., Norfolk, VA). It has a fat-mimicking ring that can be added at the periphery of the lumbar section to create a phantom that simulates a large patient. The anterior-posterior (AP) dimension of the "small" lumbar section phantom is about 19.5 cm and the lateral dimension is about 28.8 cm. The corresponding AP and lateral dimensions of the "large" lumbar section phantom (with the fat ring) are about 26.5 and 37.2 cm, respectively. A picture of this phantom in both its small and large body configurations is shown in Fig. 1, below. We utilized five custom vertebral inserts in our studies with the CIRS phantom. The inserts are made of tissue simulating epoxy resins. Two of the inserts were fat and fat-free red marrow. These

FIG. 1. Pictures of custom CIRS lumbar simulator phantom in its small (left) and large (right) body size configurations with five custom vertebral inserts.

are labeled 0/100 and 0/0, respectively, where the numerator in the label is the mg/cc of simulated bone and the denominator is the volume percent simulated fat. The remaining inserts were 100 mg/cc bone (100/0), 200 mg/cc bone (200/0), and 300 mg/cc bone (300/0) all in simulated fat-free red marrow.

II.B. Image acquisition

For the 20 cm diameter Catphan 600 and the small CIRS lumbar section phantoms, the GE Discovery CT750 HD CT scanner was operated in GSI-11 (gemstone spectral imaging 11) mode with techniques of 80 and 140 kVp at 600 mA, medium scan field of view (SFOV), eight contiguous 5 mm slices (40 mm total collimation), 0.8 s gantry rotation time, a displayed CTDIw of 26.27 mGy, and a displayed field of view (DFOV) of 25 cm for the Catphan and 36 cm for the small CIRS lumbar section phantom. (Note, at the time of this study, the GE scanner offered 18 GSI body scan modes with either medium or large SFOV, 20 or 40 mm total collimation, 600–640 mA, 0.5–1 s gantry rotation time, and CTDIw values of 17.49–36.34 mGy; all utilize switching between 80 and 140 kVp). According to Li *et al.*,[28] the flux ratio between low and high kVp is optimized for the CT750 HD scanner with a distribution of scan times of 65% at 80 kVp and 35% at 140 kVp. Using this time distribution and the relative CTDIw values for the scanner at 80 and 140 kVp (6.49 mGy at 80 kVp vs 27.43 mGy at 140 kVp, both at 240 mAs), it can be computed that 30.5% of the dose is obtained at 80 kVp and 69.5% of the dose is obtained at 140 kVp. For the 32 cm diameter Gammex 467 phantom and the large CIRS lumbar section (with the fat ring), the scanner was operated in the GSI-10 mode, with techniques of 80 and 140 kVp at 600 mA, large body SFOV, 8 contiguous 5 mm slices, 0.8 s gantry rotation time, a displayed CTDIw of 25.13 mGy, and DFOVs of 40 cm for the 467 phantom and 50 cm for the large CIRS lumbar section phantom. Conventional polyenergetic CT images of the small and large CIRS lumbar sections were generated for comparison with the dual energy synthesized monochromatic images of these phantoms. The technique factors that were employed for the conventional images were 80, 120, and 140 kVp, 8 contiguous 5 mm slices, 400 mA, 1 s for the small CIRS phantom and 250 mA, 2 s for the large CIRS phantom.

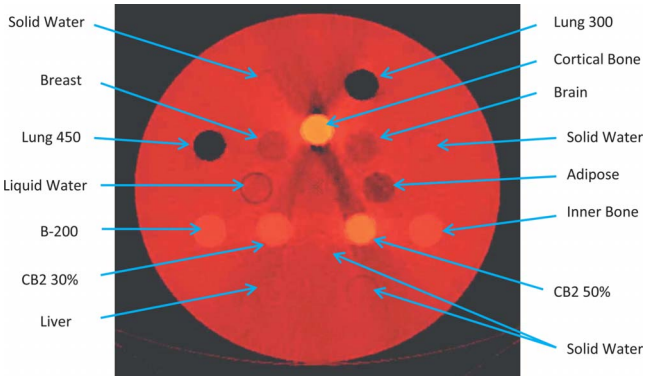

FIG. 2. Effective atomic number map of the Gammex 467 phantom showing the locations of all inserts. Pixel values in this image are in units of atomic number. Effective atomic numbers are determined from this map using circular regions of interest.

The scanner was operated in axial mode in all cases. The scans were repeated three times for each condition to test reproducibility. The middle slices (fourth of the eight contiguous 5 mm slices) for the three acquisitions for each condition were analyzed in all cases. The GE GSI-viewer was employed to display the effective atomic number maps and synthesized monochromatic CT images. The mean CT numbers and Z_{eff} were measured using regions of interest (ROIs)

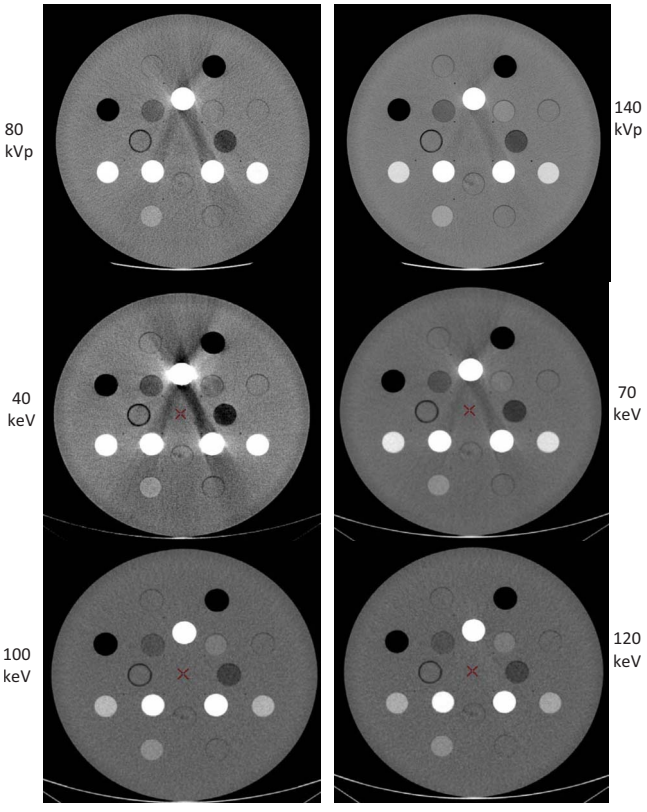

FIG. 3. Polyenergetic and synthesized monochromatic CT images of the Gammex 467 phantom. Note that there are significant streak artifacts in the 80 kVp polyenergetic and 40 and 70 keV monochromatic images but not in the 100 and 120 keV monochromatic images. The window width was 500 HU and the window level was 50 HU for the display of each of these images.

TABLE I. Measured vs true effective atomic numbers of inserts in the Gammex 467 phantom. [Note: The Z_{eff} for the lung inserts could not be measured with the CT scanner (measured Z_{eff}=0), so these are not included in the table.]

	Adipose	BR12 breast	Solid Water 11 o'clock	LV1 liver	SR2 brain	IB3 inner bone	B200 bone mineral	CB2 30%	CB2 50%	SB3 cortical bone	Liquid Water	Solid Water 2 o'clock	Solid Water 6 o'clock	Solid Water 5 o'clock
True Z_{eff}	6.40	7.24	8.11	8.11	6.31	10.90	10.90	11.39	12.98	14.02	7.42	8.11	8.11	8.11
Average measured Z_{eff}	6.36	7.50	8.02	7.65	7.26	10.53	10.52	11.00	12.48	13.52	7.83	8.05	8.01	7.71
Measured Z_{eff}–true Z_{eff}	−0.05	0.26	−0.09	−0.46	0.95	−0.37	−0.38	−0.40	−0.50	−0.49	0.41	−0.06	−0.10	−0.40
Measured/true Z_{eff}	0.99	1.04	0.99	0.94	1.15	0.97	0.97	0.97	0.96	0.96	1.06	0.99	0.99	0.95
Measured Z_{eff} COV (%)	0.78	0.66	0.26	0.30	0.32	0.40	0.31	0.26	0.05	0.24	0.38	0.54	0.63	0.65

that were large enough to provide good statistics, but sufficiently inside the outer edges of the objects of interest to avoid volume averaging. The sizes of the ROIs were 290 mm^2 for the Gammex 467 phantom, 55 mm^2 for the Catphan, and 180–190 mm^2 for the CIRS lumbar simulator phantoms.

II.C. True monochromatic CT numbers and effective atomic numbers

The true effective atomic numbers (Z_{eff}) for the inserts in the Gammex 467 phantom were supplied by Gammex. Those for all of the plastics in the Catphan phantom except PMP were from a paper by Phelps *et al.*,[29] who computed the values using Mayneord's equation.[30] We employed Mayneord's equation [Eq. (4), below] to compute the effective atomic number of PMP ($C_6H_{12}(CH_2)$),

$$Z_{eff} = \sqrt[2.94]{f_1 Z_1^{2.94} + f_2 Z_2^{2.94} + \ldots}, \quad (4)$$

where f_i is the fraction of electrons in element i and Z_i is the atomic number of element i.

The true CT numbers of the inserts in the phantoms were computed from the mass attenuation coefficients determined with the NIST XCOM computer program,[31,32] and from the mass densities supplied by the manufacturers. The chemical formulas of the plastic inserts in the Catphan and the mass fractions of the elements in the tissue substitute inserts of the Gammex 467 phantom, as supplied by the manufacturer, were entered into XCOM for the computation of the total mass attenuation coefficients of the inserts. The equation employed to compute the true CT numbers of the inserts in both phantoms was

$$\mathrm{CT\#}_i(E) = 1000 * \left[\frac{(\mu/\rho)(E)_i \cdot \rho_i - (\mu/\rho)(E)_{\mathrm{water}} \cdot \rho_{\mathrm{water}}}{(\mu/\rho)(E)_{\mathrm{water}} \cdot \rho_{\mathrm{water}}} \right], \quad (5)$$

where $(\mu/\rho)(E)_i$ is the mass attenuation coefficient of insert i at energy E, $(\mu/\rho)(E)_{\mathrm{water}}$ is the mass attenuation coefficient of water at energy E, ρ_i is the mass density of insert i as supplied by the manufacturer, and ρ_{water} is the density of water at room temperature (0.99823 g/cc at 20 °C). Both measured and computed CT numbers were obtained at monochromatic energies of 40–120 keV in increments of 10 keV.

We queried the manufacturer of the Catphan as to the accuracies of the mass densities of the plastic rods in their linearity section that are listed in the Catphan 500–600 manual. The manufacturer responded that there can be a small uncertainty in the second digit after the decimal point. We therefore decided to include in our study an investigation of the effects of variations in the assumed true mass densities within a range of the nominal densities (ND) ±0.02 g/cc on the comparisons between the true and measured CT numbers. The densities for each material were incremented by 0.001 g/cc within these ranges for the true CT number calculations.

III. RESULTS

An example of the effective atomic number map of the Gammex 467 phantom is shown in Fig. 2. The average measured Z_{eff} values for the inserts in the Gammex 467 phantom are compared to the true values in Table I and those for the Catphan are listed in Table II. The coefficients of variation of

TABLE II. Measured vs true effective atomic numbers of plastic inserts in the linearity section of the Catphan.

	Teflon	Delrin	Acrylic	Polystyrene	LDPE	PMP
Molecular formula	CF_2	$(OCH_2)_n$	$C_5H_8O_2$	C_8H_8	C_2H_4	$C_6H_{12}(CH_2)$
True Z_{eff}	8.43	6.95	6.47	5.69	5.44	5.44
Average measured Z_{eff}	8.80	7.03	6.48	5.09	4.66	4.64
Measured Z_{eff}–true Z_{eff}	0.37	0.08	0.01	−0.60	−0.78	−0.80
Measured/true Z_{eff}	1.04	1.01	1.00	0.89	0.86	0.85
Measured Z_{eff} COV (%)	0.24	0.62	0.09	0.79	2.05	1.08

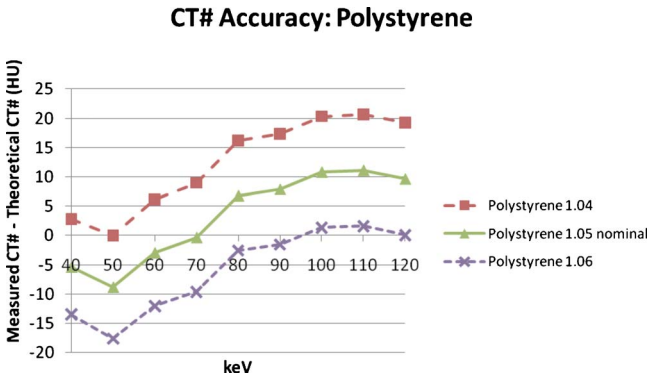

FIG. 4. Measured–theoretical (true) CT numbers at 40–120 keV for the polystyrene rod in the Catphan phantom. The differences are shown for true CT numbers computed with the ND (1.05 g/cc) and the nominal ±0.01 g/cc. The minimum RMS error between the measured and true CT numbers for the 40–120 keV range was 7.06 HU, which was obtained for an assumed true mass density of 1.054 g/cc, which is nearly identical to the nominal mass density (1.05 g/cc) in this case (RMS error for ND =7.87 HU).

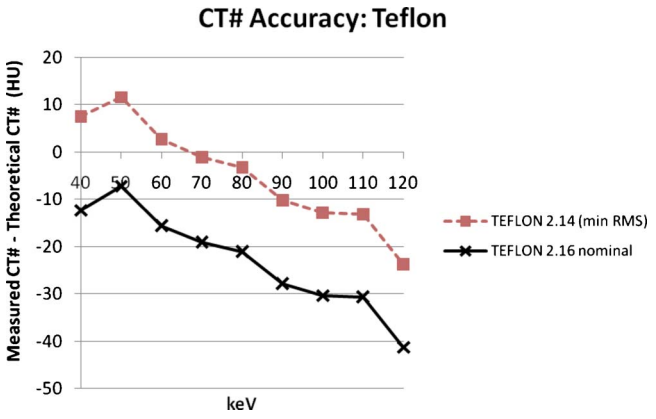

FIG. 6. Measured–theoretical (true) CT numbers at 40–120 keV for the Teflon rod in the Catphan phantom. The CT number differences are shown for true CT numbers computed with the nominal mass density (2.16 g/cc) and the nominal density −0.02 g/cc for which the minimum RMS error between the measured and true CT numbers was obtained in the analyzed (ND ± 0.02 g/cc) density range.

the measured Z_{eff} values for three different scans are also listed in these tables.

Polyenergetic (80 and 140 kVp) and synthesized monochromatic (40, 70, 100, and 120 keV) CT images of the Gammex 467 phantom are shown in Fig. 3, above. Plots comparing the measured monochromatic CT numbers with the true monochromatic CT numbers at various assumed true physical densities are shown in Figs. 4–6 for several Catphan phantom plastic rods and in Figs. 7–9 for several Gammex 467 phantom tissue mimicking inserts.

Table III lists the RMS errors between the measured and true monochromatic CT numbers from 40 to 120 keV for the Catphan plastics when the true CT numbers are computed using the nominal densities of the plastics. Also listed are the minimum RMS errors that are obtained when the true CT numbers are computed using densities in the range of the nominal densities ±0.02 g/cc.

Table IV lists the RMS errors of the synthesized monochromatic CT numbers of the inserts in the Gammex 467 phantom. The measured and true CT numbers of the entire sets of inserts in the phantoms can also be compared at individual monochromatic energies. An example of such a comparison at 90 keV for the inserts in the Gammex 467 phantom is displayed in Fig. 10, where the error (measured CT#– true CT#) is plotted on the ordinate, and the true CT# on the abscissa.

Plots at other keV are similar, but the errors are larger. Specifically, the RMS errors between the measured and true CT numbers for the entire set of inserts in the Gammex 467 phantom as a function of keV [assuming nominal densities for the true CT numbers] are 189, 93, 55, 39, 30, 26, 28, 27, and 29 HU at 40, 50, 60, 70, 80, 90, 100, 110, and 120 keV, respectively.

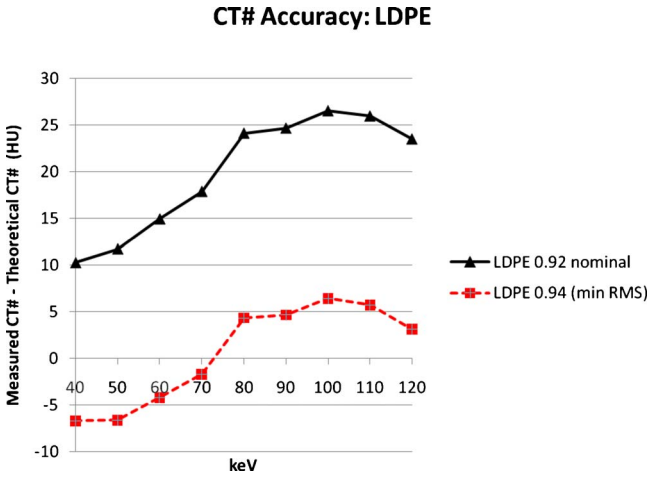

FIG. 5. Measured–theoretical (true) CT numbers at 40–120 keV for the LDPE rod in the Catphan phantom. The CT number differences are shown for true CT numbers computed with the nominal mass density (0.92 g/cc) and the nominal density +0.02 g/cc for which the minimum RMS error between the measured and true CT numbers was obtained in the analyzed (ND ± 0.02 g/cc) density range.

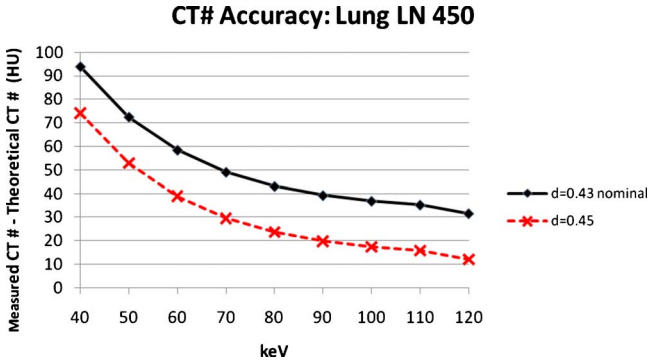

FIG. 7. Measured–theoretical (true) CT numbers at 40–120 keV for the lung LN 450 insert in the Gammex 467 phantom. The CT number differences are shown for true CT numbers computed with the nominal mass density (0.43 g/cc) and the nominal density +0.02 g/cc for which the minimum RMS error between the measured and true CT numbers was obtained in the analyzed (ND ± 0.02 g/cc) density range.

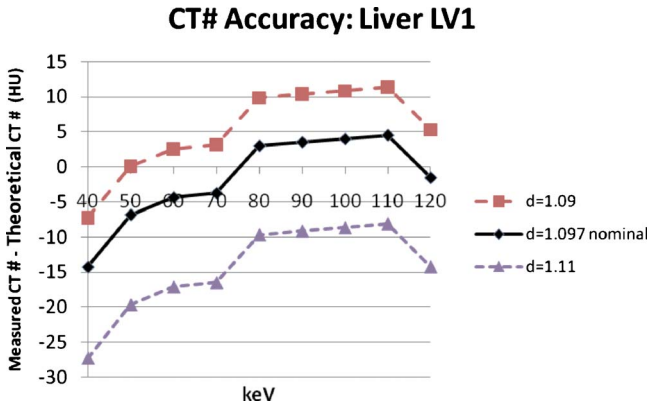

FIG. 8. Measured−theoretical (true) CT numbers at 40–120 keV for the liver LV1 insert in the Gammex 467 phantom. The CT number differences are shown for true CT numbers computed with the nominal mass density (1.097 g/cc) and with the nominal density ±0.01 g/cc. The RMS error between the measured and true CT numbers for the nominal density was within 0.3 HU of the minimum RMS error obtained for this insert.

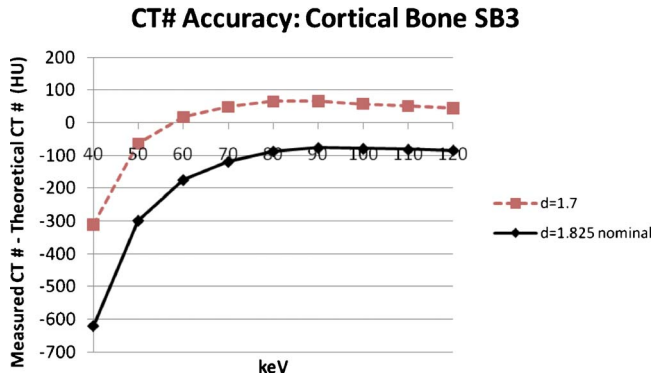

FIG. 9. Measured−theoretical (true) CT numbers at 40–120 keV for the cortical bone SB3 insert in the Gammex 467 phantom. The CT number differences are shown for true CT numbers computed with the nominal mass density (1.825 g/cc), for which the RMS error is 248 HU and for a much greater variation in the assumed mass density than was used for other inserts (−0.125 g/cc) for which the RMS error is still very large (115 HU).

A comparison of the effects of body size on the CT numbers in conventional polyenergetic CT imaging and synthesized monochromatic CT imaging, using the CIRS lumbar section phantom, is shown in Fig. 11. The differences between the CT numbers of vertebral inserts within the small and large lumbar sections are plotted at various kVp for conventional imaging in part (a) of this figure, and at various keV for the dual energy synthesized monochromatic images in part (b) of this figure.

IV. DISCUSSION

IV.A. Effective atomic numbers

Although the effective atomic numbers of the lung simulating materials could not be measured with the dual energy technique, the measured effective atomic numbers of all of the other materials in both the Catphan and the Gammex 467 phantoms were accurate to within 15%. The largest (−15%) errors were obtained for materials with effective atomic numbers less than 6.4 in both phantoms. The errors for the other materials ranged from −6% to +6%. These errors are comparable to those that were obtained by Bazalova *et al.* in their study of "dual energy CT-based material extraction" in which they used a similar Gammex 467 phantom.[26] They employed a numerical dual energy CT approach to solve for the effective atomic numbers of the materials in this phantom. This approach required the input of the measured 100 and 140 kVp spectral distributions corrected for beam hardening, measured CT numbers of the materials at 100 and 140 kVp, and NIST attenuation coefficients for elements having atomic numbers between 5 and 15, which is the range within the Gammex phantom. From Fig. 6 of their paper, the errors ranged from about −6% to +5% with an outlier at 12%. The latter was obtained for CB3 resin, the composition of which they believed had changed with time. Our effective atomic number results are also comparable to those of Rutherford *et al.*, who employed an iterative numerical technique and obtained an accuracy of about 3%, with lesser accuracy at low Z (<6) and high Z (>12) values.[2,3] Finally, our results are comparable to those of Heismann *et al.*, who employed a numerical density-atomic number (ρZ) method and obtained an accuracy of about 4% for chemical solutions having effective atomic numbers in the 7.2–9.8 range, with the greatest error (4%) at the maximum effective atomic number.[33]

One of the first applications of the use of measured effective atomic numbers with dual energy CT was in the characterization of brain lesions such as colloid cysts, dermoid cysts, and meningiomas.[2] In these cases, the measured effective numbers were combined with the measured electron

TABLE III. RMS errors (HU) between the measured and true monochromatic CT numbers of the Catphan plastics in the 40–120 keV range, including the effect of deviations in the assumed mass densities of the plastics.

	Teflon	Delrin	Acrylic	Polystyrene	LDPE	PMP
ND (g/cc)	2.16	1.41	1.18	1.05	0.92	0.83
RMS error for ND (HU)	24.95	13.81	13.68	7.87	20.85	20.37
Minimum RMS error (HU)[a]	11.61	3.59	4.81	7.06	5.10	4.66
Density for minimum RMS error (g/cc)	2.14	1.424	1.19	1.054	0.94	0.85
Density for minimum RMS error−ND (g/cc)	−0.02	0.014	0.01	0.004	0.02	0.02

[a]Minimum for set of RMS errors obtained using ND and densities in the range of ND ±0.02 g/cc for computation of true CT numbers.

densities for improved characterization. Similarly, in a recent paper, Mahnken *et al.*[34] employed the dual energy CT ρZ method of Heismann *et al.*[35] to characterize body fluids *ex vivo*. They found the ρZ method to be superior to attenuation based assessment (e.g., plotting 80 kVp CT numbers vs 140 kVp CT numbers) at differentiating blood, mixtures of blood, and pus samples.[34]

According to Heismann *et al.*, "an accuracy of 0.1 to 0.2 is required for Z_{eff} to permit reliable fluid and soft tissue identification."[33] The differences between the measured and true Z_{eff} that we obtained with the GE CT750 HD scanner in our study (Tables I and II) were, in many cases, considerably greater than 0.2. Rutherford *et al.*[3] found that substantial improvement in the accuracies of the measured effective atomic numbers could be obtained with dual energy CT techniques that employed "beam energies which are further apart." Their study, which also took x-ray dose into consideration, indicated that "if energies of 40 and 80 keV are employed, a precision of at least 1 part in 400 in the measurement of effective atomic number can be achieved."[3] Mahnken *et al.*[34] achieved the 0.1–0.2 effective atomic number accuracy recommended by Heismann[35] by filtering their 80 kVp spectrum with 0.6 mm titanium and their 140 kVp spectrum with 1.2 mm titanium. Others have found optimal combinations of 80 kVp with Tb/Hf and 140 kVp with Bi/Mo filter pairs[36] and 80 kVp with standard CT filtration, 140 kVp with standard CT filtration plus either 0.5 mm tin for large patients, or 0.8 mm tin for normal size patients.[19] While differential filtering similar to the above for improved spectral separation is not presently possible with the rapid kVp switching dual energy CT scanner, it may be developed in the future. Differential spectral filtering has been incorporated in dual-source dual energy CT scanners;[19] however, these scanners have other attributes that can negatively impact accuracy including the detection of cross scatter, the employment of a postreconstruction image based dual energy method that is more subject to beam hardening errors, and the substantial physical displacement between the projections acquired at the low and high kVp's that can result in greater discrepancies in the dual energy data as a result of motion.

IV.B. Synthetic monochromatic CT images and CT numbers

The synthesized monochromatic CT images displayed in Fig. 3 indicate that these images are not truly monochromatic as there are substantial streaking artifacts surrounding the cortical bone insert. These artifacts are much more prevalent in the lower keV images than in the higher keV images. Had the synthesized images truly been monochromatic, the phantom/patient size would have had no effect on CT numbers, and the CT numbers of the vertebral inserts in the small and large lumbar section CIRS phantoms would have been the same. Figure 11(b) indicates that the differences especially at low keV's were substantial. For example, in the 40 keV monochromatic images, the difference between the CT numbers of the 300 mg/cc bone in red marrow (300/0) insert in the small and large phantoms was 47 HU. The correspond-

TABLE IV. RMS errors (HU) between the measured and true monochromatic CT numbers of the Gammex 467 tissue simulating inserts in the 40–120 keV range, including the effect of deviations in the assumed mass densities of the inserts.

	Lung LN300	Lung LN450	Adipose AP6	Breast BR12	Solid Water 11 o'clock	Liver LV1	Brain SR2	Inner bone IB3	Bone mineral B200	CB2 30%	CB2 50%	Cortical Bone SB3	Liquid Water	Solid Water 2 o'clock	Solid Water 6 o'clock	Solid Water 5 o'clock
ND (g/cc)	0.29	0.43	0.942	0.977	1.017	1.097	1.053	1.143	1.154	1.335	1.56	1.825	0.9982	1.017	1.017	1.017
RMS error for ND (HU)	46.74	54.72	17.42	26.81	15.16	6.19	41.77	25.45	26.84	52.87	140.90	248.0	10.12	14.83	9.14	5.60
Minimum RMS error (HU)[a]	32.46	37.07	6.56	16.53	7.30	5.92	33.91	17.35	19.44	34.54	118.10	169.0	9.12	7.76	7.13	3.85
Density for minimum RMS error (g/cc)	0.31	0.45	0.959	0.997	1.031	1.095	1.073	1.126	1.138	1.315	1.54	1.805	1.0022	1.030	1.023	1.021
Density for minimum RMS error−ND (g/cc)	0.02	0.02	0.017	0.02	0.014	−0.002	0.02	−0.017	−0.016	−0.02	−0.02	−0.02	0.004	0.013	0.006	0.004

[a]Minimum for set of RMS errors obtained using ND, and densities in the range of ND ± 0.02 g/cc for computation of true CT numbers.

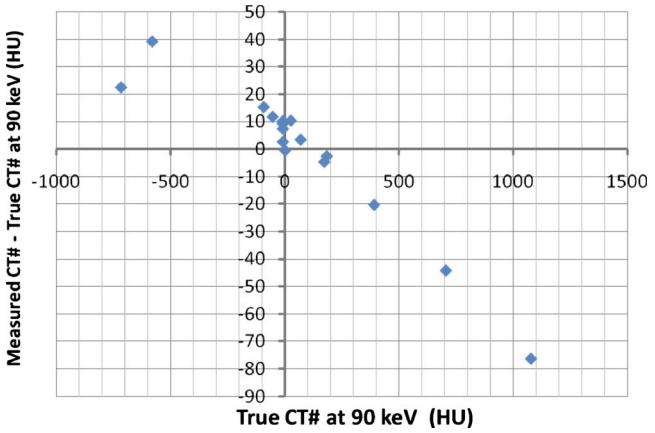

FIG. 10. Plot of the error in the measured CT numbers of the inserts in the Gammex 467 phantom at 90 keV as a function of the true CT numbers at 90 keV. (The true CT numbers were computed using the nominal densities of the inserts for this plot.)

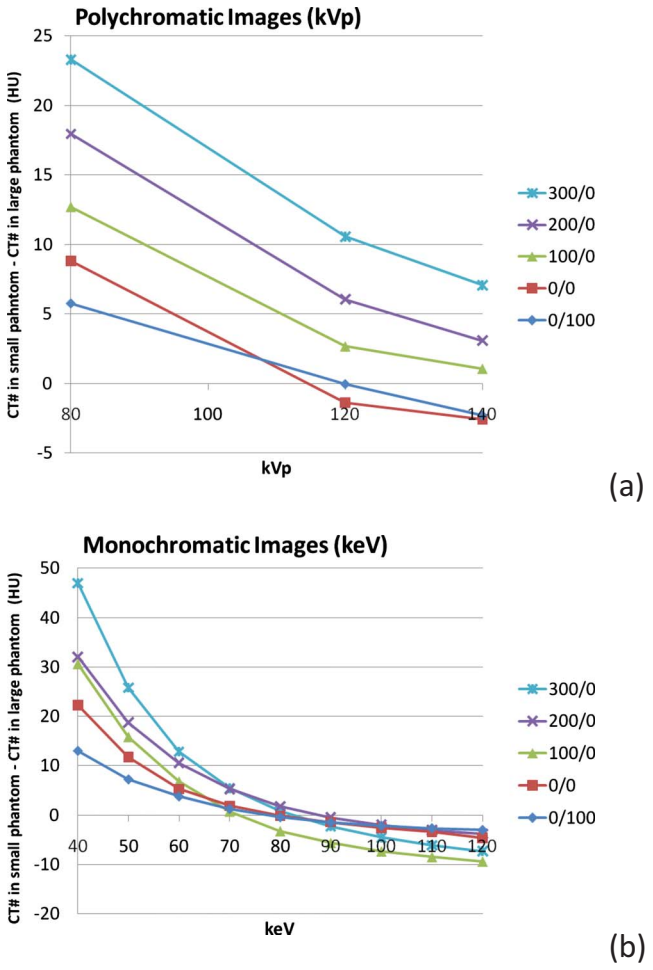

FIG. 11. Differences between the CT numbers obtained when individual vertebral inserts were scanned within the small and large CIRS lumbar sections both conventionally at 80, 120, and 140 kVp (a) and with dual energy (b). For the latter, the differences are calculated at synthesized monochromatic energies of 40, 50, 60, …, 120 keV. The numerators in the labels for the inserts indicate the mg/cc of the simulated bone and the denominators indicate the volume percent of the simulated fat. For example, 300/0 is a 300 mg/cc bone in a fat-free red marrow insert and 0/100 is a 100% fat insert with 0 mg/cc bone.

ing CT number difference for conventional polyenergetic CT imaging of the phantoms at 80 kVp [Fig. 11(a)] was about half as great (23 HU). At higher monochromatic and polyenergetic energies, the differences in CT numbers due to the size of the phantoms diminished significantly, and, in some cases, reversed sign. Using the same 300/0 insert as an example, the difference between the CT numbers of this insert in the small and large phantoms decreased from 47 HU at 40 keV to 5 HU at 70 keV and to −4 HU at 100 keV. For polyenergetic CT imaging, the differences between the CT numbers in the small and large phantoms decreased from 23 HU at 80 kVp to 11 HU at 120 kVp and 7 HU at 140 kVp.

As shown in Tables III and IV and Figs. 5–7, even small changes in the assumed true mass densities that are used to compute the true CT numbers of materials can have a major impact on the comparisons between the measured and true CT numbers. From Table III, changes in mass density within a range of the nominal density ±0.02 g/cc can reduce the RMS errors between the true and measured monochromatic CT numbers of inserts in the Catphan phantom for a 40–120 keV range by up to a factor of 4.4. The corresponding effect in the Gammex 467 phantom (Table IV) is a reduction in the RMS error by up to a factor of 2.7.

The plots of the accuracies of the monochromatic CT numbers as a function of energy for the various materials studied had four basic shapes. For example, the plots for PMP, LDPE, polystyrene, and LV1 (Figs. 4, 5, and 8) had sinusoidal-like shapes with the minimum RMS error plots going through 0 HU error between 70 and 75 keV. For others like Teflon and lung (Figs. 6 and 7), the plots are essentially monotonically decreasing with energy, and for bone (Fig. 9), the plots are monotonically increasing. Plots for acrylic and Delrin (not shown) were sinusoidal like those for PMP, LDPE, polystyrene, and LV1, but the measured values were greater than the theoretical at low energies, with a minimum (~0 HU error) at about 60 keV.

The largest discrepancies between the measured and true monochromatic CT numbers occurred for the very low density and high density inserts. For example, using the nominal densities, the RMS errors in the Gammex 467 phantom are 47–55 HU for the lung inserts with densities of 0.29 and 0.43 g/cc, respectively, and 53, 141, and 248 HU for bone mixtures CB2 30%, CB2 50%, and cortical bone with densities of 1.335. 1.56, and 1.825 g/cc, respectively. The RMS errors for the other inserts are typically less than 27 HU when the nominal density is employed to compute the true CT numbers and less than 20 HU when a density in the range of nominal density ±0.02 g/cc is used that minimizes differences. The one exception is brain SR2, which has a relatively large RMS error of 41.8 HU at nominal density. This insert has a medium density (1.053 g/cc), but a low atomic number (6.42). The latter would result in a low probability of photoelectric interactions, which appears to negatively impact both the monochromatic CT number accuracy and the effective atomic number accuracy (error of 15%, Table I) of the dual energy measurements with this scanner.

In their research with an early rapid kVp switching dual energy CT scanner, Montner *et al.*[16] found that the errors in the measured CT numbers depended on both the material being imaged and the monochromatic energy of the synthesized image. As shown in Figs. 4–9, our results show similar effects. The minimum overall errors that we obtained for the synthesized monochromatic images of the Gammex 467 phantom were at 90 keV (assuming nominal densities). As shown in Fig. 10, for a range of true CT numbers between −100 and 400 HU, the error in the measured CT numbers is between −20 and +20 HU, and much larger errors occur outside this range. The errors that we observed are, in general, larger than those obtained by Montner *et al.* (e.g., from about −15 to +8 HU for true CT numbers in the −200–750 HU range at 80 keV), but the majority of the measurements of Montner *et al.* were made with scans of 12 cm diameter hollow cylindrical phantoms that were filled with homogenous chemical solutions.[16] Errors due to scatter and beam hardening would be much less with such small phantoms. Also, the use of separate phantoms for each chemical solution makes the results immune to the influences of streaking that can arise from very attenuating (e.g., cortical bone) inserts at other locations within phantoms like the Gammex 467 phantom.

Theory predicts that prereconstruction basis material decomposition methods eliminate spectral beam hardening artifacts.[4,5,14] However, these methods do not inherently eliminate the effects of x-ray scatter. Therefore, the variations in the measured monochromatic CT numbers with phantom size that we observed are likely due to scatter. The effect of scatter on dual energy CT material density images was studied by Vetter and Holden.[37] They measured scatter fractions for a Siemens Somatom DR3 CT scanner and found the scatter fractions varied from about 2% for a 20 cm Plexiglas phantom to about 4% for a 25 cm Plexiglas phantom with 3 cm aluminum. By applying corrections based on their scatter measurements to basis material lookup tables, Vetter and Holden addressed nonlinearities in the lookup tables due to scatter and were able to improve the accuracies of their basis material densities for both low and high Z basis materials. The Somatom scanner that they employed had a maximum slice thickness/collimation width of 10 mm; whereas modern multidetector scanners like the GE CT750 HD have total collimation widths of 20–40 mm or more, which should result in higher scatter fractions that may be more difficult to correct. A 40 mm total collimation width was employed in all of the studies described in Sec. II.

IV.C. Additional studies of phantom size and collimator width

To better understand the effects of phantom size and collimator width on the DECT results obtained with the GE CT750 HD CT scanner, we performed additional studies. First, Teflon and acrylic rod inserts (~2.6 cm in diameter) for an RMI model 460 CT head phantom (Gammex-RMI, Middleton, WI) were scanned by themselves (referred hereafter as configuration A) at the center of the SFOV. The rods were then individually placed within a small tapered Solid Water holder (diameter of ~4.8 cm in the scan region) and again scanned at the center of the SFOV (configuration B). Finally, the tapered Solid Water holder with the rod was placed in the central insert position of the 19.8 cm diameter RMI model 460 phantom (configuration C), which was centered in the SFOV and scans were performed. The RMI phantom is made of Solid Water and includes a 0.4 cm thick cortical bone rim. Images of the Teflon rod in configurations A–C are shown in Fig. 12, above.

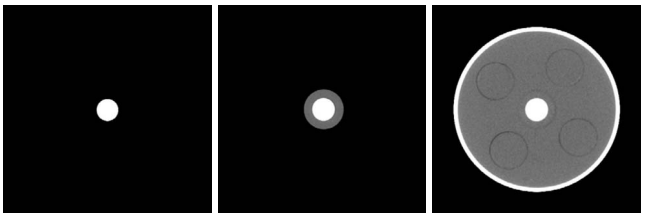

FIG. 12. CT images of the Teflon rod by itself in configuration A (left), in a Solid Water holder in configuration B (middle), and within an RMI head CT phantom in configuration C (right).

The measured Z_{eff} and monochromatic CT numbers most closely matched the theoretical values when the Teflon and acrylic rods were scanned within the RMI head phantom. The measured minus the true effective atomic numbers were −1.18, −0.97, and −0.01 for the acrylic rods in configurations A, B and C, respectively. The corresponding differences for the Teflon rod were 0.29, 0.36, and 0.29. The RMS errors of the measured minus the true CT numbers in the 40–120 keV range with 10 keV increments (assuming nominal mass densities for the true CT numbers) were 24.7, 21.1, and 11.0 HU for the acrylic rod in configurations A, B, and C, respectively. The corresponding RMS errors for the Teflon rods were 10.9, 12.7, and 7.6 HU. These results appear to contradict our hypothesis that the observed variations in monochromatic CT numbers with phantom size in our original experiment may be due to x-ray scatter since the minimum errors in the measured CT numbers in this additional experiment were obtained for the configuration (C) that had the maximum amount of scatter. However, the results could also be explained by that fact that the objects in configurations A and B may be considerably smaller than any considered in the calibration and x-ray scatter corrections of the DECT method for this scanner. Thus, the results might be interpreted to indicate that the calibration and x-ray scatter corrections for this scanner were generated using a phantom configuration that more closely matches configuration C, and any significant deviations from that configuration can result in substantial errors in the measured effective atomic numbers and monochromatic CT numbers. It is interesting to note that the RMS error between the measured and theoretical CT numbers of the Teflon rod in the RMI phantom (7.6 HU) was significantly less than the RMS errors for the Teflon cylinder in the Catphan (24.95 HU, Table III). One possible explanation is that the composition and density of the Teflon in the RMI phantom more closely matched the assumed composition and density for the theoretical calculations.

We performed a second study using only configuration C, but compared the results for corresponding 5 mm slices obtained with 20 and 40 mm total collimation. The use of the smaller 20 mm collimation with the concomitant lower scatter fraction had little effect on the measured effective atomic numbers (decrease of 0.01 for both acrylic and Teflon), but improved the RMS errors between the measured and theoretical CT numbers by 3.9 HU for acrylic and 2.4 HU for Teflon. The greater scatter for the 40 mm collimation should result in the appearance of less attenuation and therefore lower CT numbers. This was true for Teflon for which the average measured CT number in the 40–120 keV range with 40 mm collimation was 3.4 HU less than that with 20 mm collimation. However, it was the opposite for acrylic for which the average measured CT number with 40 mm collimation was 3.7 HU greater than that for 20 mm collimation. This difference for low Z (acrylic) and high Z (Teflon) materials may be related to an effect described by Vetter and Holden that, "using calculated tables, low Z basis material thicknesses will be underestimated in the presence of scatter, and high Z basis material thicknesses will be overestimated."[37]

IV.D. Reproducibilities of the effective atomic numbers and synthetic monochromatic CT numbers

This new CT scanner was found to be highly stable. The short term reproducibilities of the effective atomic numbers were 1.0% in the Catphan and 0.5% in the Gammex 467 phantoms. Excluding the inserts and rods for which the mean CT numbers were close to 0 HU and therefore the coefficients of variation (standard deviation/mean) were large, the coefficients of variation for the monochromatic CT numbers were about 0.8% for the Catphan and 2.4% for the Gammex 467 phantom.

V. SUMMARY AND CONCLUSION

Our initial tests indicate that the effective atomic numbers computed with the GE CT750 HD scanner in dual energy mode have accuracies (from −6% to +6% for $Z_{eff} > 6.3$) that are similar to those obtained by other investigators with different dual energy CT scanners. The accuracies of the synthesized monochromatic CT numbers obtained with this scanner depend not only on the energy and material but also on small changes in the assumed mass densities used for calculation of the true CT numbers. For the 40–120 keV range, the RMS errors between the measured and true CT numbers of the plastics in a Catphan phantom are 8–25 HU when the true CT numbers are computed using the nominal plastic densities. These RMS errors improve to 3–12 HU for assumed true densities within a nominal density (ND) ± 0.02 g/cc range. The corresponding RMS errors between the measured and true CT numbers of the tissue mimicking materials in a Gammex 467 phantom vary from about 6–248 HU for the ND and improve to 4–169 HU for assumed densities within the ND ± 0.02 g/cc range.

The synthesized monochromatic CT numbers can be very inaccurate, especially for dense tissue mimicking materials at low energies. Furthermore, the synthesized monochromatic CT numbers of materials still depend on the amount of the surrounding tissues especially at low energies, demonstrating that the numbers are not truly monochromatic. Others have shown that adding x-ray attenuating filters to increase the spectral separation between the low and high energy x-ray beams can improve the accuracy of dual energy CT measurements.[3,19,34,36] Incorporation of improved scatter correction algorithms can also be helpful, as can use of "conic and cubic surface equations to directly approximate the dual energy log-signal surface equations, and especially their inverses," which increases the accuracy of basis material decomposition[38] and therefore the resulting synthesized monochromatic CT numbers. It is hoped that some or all of these methods will be implemented in the future to improve the accuracy and therefore the tissue characterization capabilities of dual energy CT imaging with this and other CT scanners.

[a]Author to whom correspondence should be addressed. Electronic mail: goodsitt@umich.edu; Telephone: 734-936-7474; Fax: 734-232-5877.

[1]G. N. Hounsfield, "Computerized transverse axial scanning (tomography): Part 1. Description of system," Br. J. Radiol. **46**, 1016–1022 (1973).
[2]R. A. Rutherford, B. R. Pullan, and I. Isherwood, "Measurement of effective atomic number and electron-density using an EMI scanner," J. Neuroradiol. **11**, 15–21 (1976).
[3]R. A. Rutherford, B. R. Pullan, and I. Isherwood, "X-ray energies for effective atomic number determination," J. Neuroradiol. **11**, 23–28 (1976).
[4]R. A. Brooks, "A quantitative theory of the Hounsfield unit and its application to dual energy scanning," J. Comput. Assist. Tomogr. **1**, 487–493 (1977).
[5]R. E. Alvarez and A. Macovski, "Energy-selective reconstructions in x-ray computerized tomography," Phys. Med. Biol. **21**, 733–744 (1976).
[6]L. A. Lehmann, R. E. Alvarez, A. Macovski, W. R. Brody, N. J. Pelc, S. J. Riederer, and A. L. Hall, "Generalized image combinations in dual kVp digital radiography," Med. Phys. **8**, 659–667 (1981).
[7]R. E. Alvarez and E. Seppi, "A comparison of noise and dose in conventional and energy—Selective CT," IEEE Trans. Nucl. Sci. **26**, 2853–2856 (1979).
[8]A. Fenster, "Split xenon detector for tomochemistry in computed tomography," J. Comput. Assist. Tomogr. **2**, 243–252 (1978).
[9]R. A. Brooks and G. Di Chiro, "Split detector computed tomography. A preliminary report," Radiology **126**, 255–257 (1978).
[10]D. Drost and A. Fenster, "Experimental dual xenon detector for quantitative CT and spectral artifact correction," Med. Phys. **7**, 101–107 (1980).
[11]B. Rutt and A. Fenster, "Split-filter computed tomography: A simple technique for dual energy scanning," J. Comput. Assist. Tomogr. **4**, 501–509 (1980).
[12]S. Kappler and S. Wirth, "Comparison of dual-kVp and dual-layer CT in simulations and real CT system measurements, " *IEEE Nuclear Science Symposium/Medical Imaging Conference (NSS/MIC)*, Dresden, Germany, 19–25 October 2008 (IEEE, Piscataway, NJ, 2009), Vols. 1–9, pp. 4101–4104.
[13]L. Goshen, J. Sosna, R. Carmi, G. Kafri, I. Iancu, and A. Altman, "An iodine-calcium separation analysis and virtually non-contrasted image generation obtained with single source dual energy MDCT," *IEEE Nuclear Science Symposium/Medical Imaging Conference (NSS/MIC)*, Dresden Germany, 19–25 October 2008 (IEEE, Piscataway, NJ, 2009), Vols. 1–9, pp. 3143–3145.
[14]W. A. Kalender, W. H. Perman, J. R. Vetter, and E. Kolz, "Evaluation of a prototype dual-energy computed tomographic apparatus. I. Phantom studies," Med. Phys. **13**, 334–339 (1986).
[15]J. R. Vetter, W. H. Perman, W. A. Kalender, R. B. Mazess, and J. E. Holden, "Evaluation of a prototype dual-energy tomographic apparatus. II. Determination of vertebral bone mineral content," Med. Phys. **13**, 340–343 (1986).
[16]S. M. Montner, J. L. Lehr, and W. T. Oravez, "Quantitative evaluation of

a dual energy CT system," J. Comput. Assist. Tomogr. **11**, 144–150 (1987).
[17]T. R. Johnson, B. Krauss, M. Sedlmair, M. Grasruck, H. Bruder, D. Morhard, C. Fink, S. Weckbach, M. Lenhard, B. Schmidt, T. Flohr, M. F. Reiser, and C. R. Becker, "Material differentiation by dual energy CT: Initial experience," Eur. Radiol. **17**, 1510–1517 (2007).
[18]T. G. Flohr, H. Bruder, K. Stierstorfer, M. Petersilka, B. Schmidt, and C. H. McCollough, "Image reconstruction and image quality evaluation for a dual source CT scanner," Med. Phys. **35**, 5882–5897 (2008).
[19]A. N. Primak, J. C. Giraldo, X. Liu, L. Yu, and C. H. McCollough, "Improved dual-energy material discrimination for dual-source CT by means of additional spectral filtration," Med. Phys. **36**, 1359–1369 (2009).
[20]A. Santamaria-Pang, S. Dutta, S. Makrogiannis, A. Hara, W. Pavlicek, A. Silva, B. Thomsen, S. Robertson, D. Okerlund, D. A. Langan, and R. Bhotika, "Automated liver lesion characterization using fast kVp switching dual energy computed tomography imaging," in *Medical Imaging 2010: Computer-Aided Diagnosis*, edited by N. Karssemeijer and R. M. Summers (SPIE, Bellingham, WA, 2010) [Proc. SPIE **7624**, 76240V–76240V-10 (2010)].
[21]M. Joshi, D. A. Langan, D. S. Sahani, A. Kambadakone, S. Aluri, K. Procknow, X. Wu, R. Bhotika, D. Okerlund, N. Kulkarni, and D. Xu, "Effective atomic number accuracy for kidney stone characterization using spectral CT," in *Medical Imaging 2010: Physics of Medical Imaging*, edited by E. Samei and N. J. Pelc (SPIE, Bellingham, WA, 2010) [Proc. SPIE **7622**, 76223K–76223K-12 (2010)].
[22]C. Constantinou, J. C. Harrington, and L. A. DeWerd, "An electron density calibration phantom for CT-based treatment planning computers," Med. Phys. **19**, 325–327 (1992).
[23]C. Constantinou, F. H. Attix, and B. Paliwal, "A solid water phantom material for radiotherapy x-ray and gamma ray beam calibrations," Med. Phys. **9**, 436–441 (1982).
[24]D. R. White, C. Constantinou, and R. J. Martin, "Foamed epoxy resin-based lung substitutes," Br. J. Radiol. **59**, 787–790 (1986).
[25]D. R. White, R. J. Martin, and R. Darlison, "Epoxy resin-based tissue substitutes," Br. J. Radiol. **50**, 814–821 (1977).
[26]M. Bazalova, J.-F. Carrier, L. Beaulieu, and F. Verhaegen, "Dual-energy CT-based material extraction for tissue segmentation in Monte Carlo dose calculations," Phys. Med. Biol. **53**, 2439–2456 (2008).
[27]M. M. Goodsitt, "Conversion relations for quantitative CT bone mineral densities measured with solid and liquid calibration standards," Bone Miner. **19**, 145–158 (1992).
[28]B. Li, G. Yadava, J. Hsieh, N. Chandra, and M. S. Kulpins, "Head and body CTDIw of dual-energy x-ray CT with fast-kVp switching," in *Medical Imaging 2010: Physics of Medical Imaging*, edited by E. Samei and N. J. Pelc (SPIE, Bellingham, WA, 2010) [Proc. SPIE **7622**, 76221Y–76221Y-12 (2010)].
[29]M. E. Phelps, M. K. Gado, and E. J. Hoffman, "Correlation of effective atomic number and electron density with attenuation coefficients measured with polychromatic x rays," Radiology **117**, 585–588 (1975).
[30]W. V. Mayneord, "The significance of the roentgen," Acta of the International Union Against Cancer **2**, 271–282 (1937).
[31]M. J. Berger, J. H. Hubbell, S. M. Seltzer, J. Chang, J. S. Coursey, R. Sukumar, and D. S. Zucker, "XCOM: Photon cross sections database," NIST Standard Reference Database 8 (XGAM), http://www.nist.gov/physlab/data/xcom/index.cfm (2005).
[32]J. H. Hubbell, "Photon cross sections, attenuation coefficients, and energy absorption coefficients from 10 keV to 100 GeV, " Natl. Bur. Stand. (U.S.) Spec. Publ. No. NSRDS-NBS 29 (U.S. GPO, Washington, D.C., 1969).
[33]B. J. Heismann, B. J. Leppert, and K. Stierstorfer, "Density and atomic number measurements with spectral x-ray attenuation method," J. Appl. Phys. **94**, 2073–2079 (2003).
[34]A. H. Mahnken, S. Stanzel, and B. Heismann, "Spectral rho Z-projection method for characterization of body fluids in computed tomography: Ex vivo experiments," Acad. Radiol. **16**, 763–769 (2009).
[35]B. J. Heismann, "Atomic number measurement precision of spectral decomposition methods for CT," IEEE Nuclear Science Symposium Conference Record, Vol. 5, pp. 2741–2742, 2005 (unpublished).
[36]M. Saito, "Spectral optimization for measuring electron density by the dual-energy computed tomography coupled with balanced filter method," Med. Phys. **36**, 3631–3642 (2009).
[37]J. R. Vetter and J. E. Holden, "Correction for scattered radiation and other background signals in dual-energy computed-tomography material thickness measurements," Med. Phys. **15**, 726–731 (1988).
[38]H. N. Cardinal and A. Fenster, "An accurate method for direct dual-energy calibration and decomposition," Med. Phys. **17**, 327–341 (1990).